# Alteration of physico-chemical characteristics of coconut endocarp - Acrocomia aculeata - by isothermal pyrolysis in the range 250–550 °C

Shirley Duarte, Pin Lv, Giana Almeida, Juan Carlos Rolón, Patrick Perre

# Alteration of physico-chemical characteristics of coconut endocarp —*Acrocomia aculeata*— by isothermal pyrolysis in the range 250 to 550 °C

Shirley Duarte[a,c,*], Pin Lv[b], Giana Almeida[d], Juan Carlos Rolón[e,f], Patrick Perré[a,b]

[a] *LGPM, CentraleSupélec, Université Paris-Saclay, Plateau du Moulon, 91190 Gif-sur-Yvette, France*
[b] *LGPM, CentraleSupélec, Centre Européen de Biotechnologie et de Bioéconomie (CEBB), 3, rue des Rouges Terres, 51110 Pomacle, France*
[c] *Facultad de Ciencias Químicas, Universidad Nacional de Asunción, San Lorenzo, 2160, Paraguay.*
[d] *UMR GENIAL, AgroParisTech, INRA, Université Paris-Saclay, 91300 Massy, France*
[e] *Facultad de Ingeniería, Universidad Nacional de Asunción, San Lorenzo, 2160, Paraguay*
[f] *Visiting professor at LGPM, Centrale-Supélec, Châtenay-Malabry, 92290, France*

**Abstract**

Characteristics of the endocarp of *Acrocomia aculeata* fruit samples were evaluated before and after 2 h of isothermal pyrolysis in the range 250 to 550 °C. Differential thermogravimetric (DTG) curves from the char, obtained at 300 °C, confirm that degradation of hemicellulose and cellulose was complete and resulted in approximately 42.5% oxygen loss. The micrographs obtained from scanning electron microscopy with a field emission gun (SEM/FEG) confirmed a softened phase from the chars treated at 250 °C. The van Krevelen analysis shows that energy intensification of the sample transferred from peat to charcoal as the treatment intensity increased; this resulted in a 71% mass loss at 550 °C. The surface area of the treated sample increased exponentially with a factor of 1.2 per percentage of mass loss, from 450 °C and reached 216 $m^2/g$ at 550 °C as a consequence of the development of microporous structures. The water-vapor-sorption properties were strongly affected by the treatment, with a pronounced type V isotherm curve for the

*Corresponding author.
*Email address:* sjoamduart@gmail.com (Shirley Duarte)

char at 550 °C. These results show the evolution in chemical and structural properties of coconut endocarp during its isothermal pyrolysis. In particular, the improved char properties indicate that this material may be used as solid fuel or as raw material for the gasification process.

*Keywords:* surface area, elemental analysis, dynamic vapor sorption, coconut endocarp, pyrolysis mechanism.

---

## 1. Introduction

The South-American palm species *Acrocomia aculeata*, commonly known as mbocayá, macaw, macauba or just coconut palm, has attracted the attention of researchers in recent years, mainly for its enormous potential as a sustainable source of feedstock for biorefinery [1, 2, 3, 4].

Although *Acrocomia aculeata* is a native species of South America, its distribution spans the tropics and subtropics of Mexico and Central America as well. *Acrocomia aculeata* grows in regions that extend from Mexico to Argentina, but only in Paraguay, where 23 palm species have been identified [5], is its fruit (coconut) used commercially [6]; its many potential uses are shown in Fig. 1.

The endocarp represents about 21% of the overall residue mass generated after processing the mbocayá fruit [1]. In addition, it has higher values of fixed carbon, lignin content and energy density than other parts of the fruit [1, 7]. These characteristic properties allow us to consider endocarp as potential feedstock to produce biofuel or materials like charcoal and activated carbon for a variety of applications; the thermochemical conversions, pyrolysis and gasification, could be promising methods to accomplish this.

During pyrolysis, thermal decomposition of biomass components (cellulose, hemicellulose and lignin) takes place. In general, the char produced is expected to have higher carbon content and heating value. Its chemical structure and physical properties such as density, specific surface area, water content, and electrical conduction, changes according to the pyrolysis conditions and feedstocks [8, 9, 10].

The charateristic properties of char indicate its different uses. Some important aspects that make it suitable as a solid fuel, adsorbent or as catalyst, are its hygroscopicity and specified surface area. When planing to use the char in a gasification process, in particular to obtain activated carbon or syn-gas, its porosity, moisture content and chemical composition, are impor-

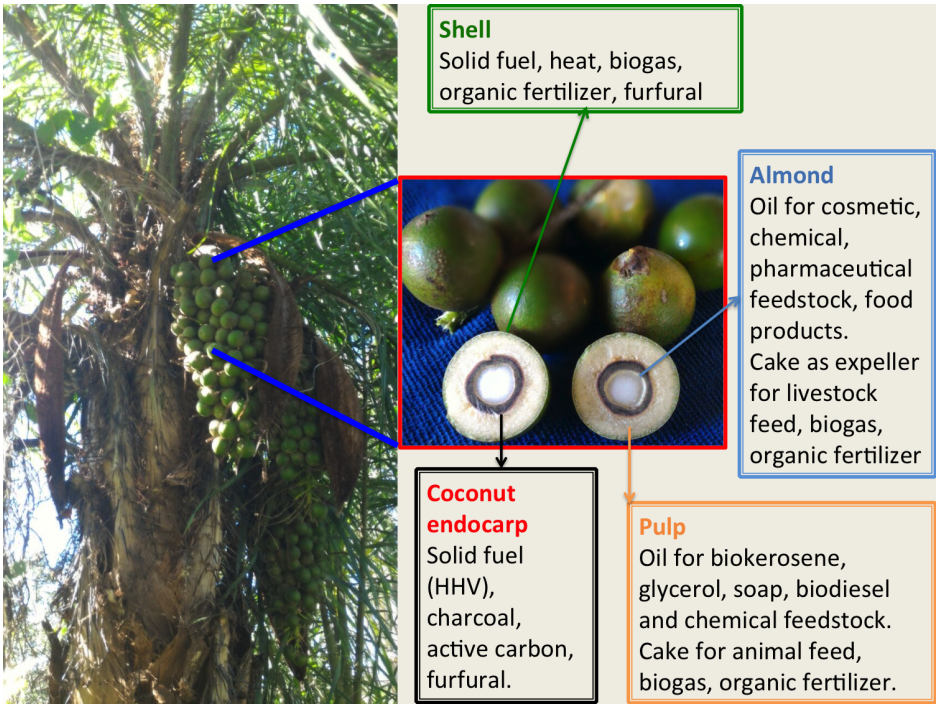


Figure 1: Potential uses of Acrocomia fruit.

tant characteristics that result from the process, to maximize a particular product.

Adsorption experiments are considered a powerful tool to study materials. In previous studies [11, 12], sorption properties were evaluated in torrefied biomass and bio-char obtained from wood samples. Natural fibers have displayed differences in water vapor sorption behavior while the hysteresis loop and its lignin contents exhibit a direct relationship [13]. New analysis has also found that a function of the elemental composition in mildly heat-treated wood can predict the occupancy of water sorption sites [14].

Though some char properties have been extensively studied [9, 10], to our knowledge, no study concerning the evolution of elemental analysis, surface area and water vapor sorption properties during pyrolysis of coconut endocarp, exists.

The important role of biomass feedstock in the pyrolysis process is well known. The composition and physical properties of the pyrolysis products depends on the raw material properties. Holocellulose and lignin content in

coconut endocarp, was determined by [1, 2] and the intense lignification of its sclereids cells, provides its impermeability and petrous consistency [2, 15].

In order to produce different fuels and chemicals from pyrolysis, the composition of raw material and thermal decomposition mechanism should be determined. Although there are extensive studies on the mechanisms of biomass pyrolysis [16, 17, 18], none is specific to this feedstock or the kinetic progress of its thermal decomposition.

In this study, mass loss as a function of time, in static conditions, were used to explain kinetic pyrolysis in the coconut endocarp. Three decomposition rates were observed from the mass loss vs time curves, related to the three main components' degradation. These measurements serves as the basis for future work in developing a kinetic model for biomasses of this type.

The major focus of this study is the experimental characterization of the coconut endocarp and its chars, obtained from a variety of isothermal pyrolysis conditions. It is important to propose the more relevant use of coconut endocarp and its chars, as *Acrocomia aculeata* is a potential feedstock for a biorefinery, likely to reduce deforestation and pollution.

The analysis techniques employed for this study included: elemental analysis, gas sorption analysis, water vapor sorption analysis, environmental and scanning electron microscopy (ESEM-FEG/SEM). In addition, the thermogravimetric TG and DTG curves, for the coconut endocarp and char samples were used as a tool for obtaining information about the main structural components degradation. From our results, coconut endocarps could be used as feedstock to produce three different products: high-quality bio-oil or solid fuel (treatment at 250 °C to 300 °C), charcoal of different quality depending upon the end use (treatment at 350 °C to 450 °C), and feedstock to a gasification process (treatment above 500 °C).

## 2. Experimental

### *2.1. Materials and pyrolysis conditions*

*Acrocomia aculeata*, indigenous to Paraguay, is usually found in areas situated between the latitudes 19 and 27 south and longitudes 54 and 62 west. The solid and woody residue inside the *Acrocomia aculeata* fruit, referred to as 'coconut endocarp", was used in this study. The availability of the coconut endocarp, as agroindustrial waste in Paraguay, is about 7 tonnes of dry matter per hectare per year [19]. The feedstock was cleaned with water

and dried in air flow at room temperature. Sample particles, between 0.2-0.63 mm selected from a previous work [7], were obtained using a grinder (IKA M20 Universal mill) and subsequently sieved.

The pyrolysis was carried out by a STA 449 F3 Jupiter, NETZSCH at atmospheric pressure. Each sample with an initial weigh of $10 \pm 2$ mg was placed in an alumina crucible and heated at 5 °C $min^{-1}$ under a nitrogen flow of 50 mL $min^{-1}$ (STP). Initially, samples were heated from ambient temperature to 100 °C, and dried for 30 minutes. The temperature was then increased to a final temperature (250 °C, 300 °C, 350 °C, 400 °C, 450 °C, 500 °C, 550 °C) and was observed, thereafter, for 2 hours.

The percentage mass loss "$ml$" defined as the instantaneous anhydrous mass loss as a function of time, was calculated with the following equation 1.

$$ml = \frac{m_i - m_t}{m_i} \times 100 \tag{1}$$

where $m_i$ is the anhydrous mass at the beginning of the thermal degradation (after they were dried at 100 °C for 30 min) and $m_t$ is the anhydrous mass of the char residue (thermal treated sample) in the instant $t$ of the thermal degradation. The final mass loss "$fml$" is measured at the end of the plateau for each selected temperature. This method was employed following previous testing in this lab which indicated that 30 min at 100 °C was enough time to release the moisture content in powder wood samples [20].

The term "char" in this study, refers to the solid residue that remains in the crucible after each treatment. This term, and its associated temperature, are used to refer to the char obtained after each pyrolysis treatment obtained at a specific temperature, for example, "350 °C-char", represents the char obtained after the pyrolysis of coconut endocarp at 350 °C for 2 h in the condition described above.

In addition, derivative thermogravimetric (DTG) curves were plotted for the cases of untreated endocarp and char samples in order to check for the characteristic DTG peaks normally found in carbohydrate decomposition (cellulose, hemicellulose and lignin). The heating rate employed was 10 °C/min under the nitrogen gas flow of 50 ml/min. The initial mass sample remained between 3 and 4 mg. All experiments were performed in triplicate and several blank tests were made to correct the effects of buoyancy forces.

### *2.2. Analytical Methods*

#### *2.2.1. Elemental analysis*

The evolution of the elemental composition was measured by Thermo Scientific FLASH 2000 CHNS/O analyzers. In order to determine carbon, hydrogen, nitrogen and sulfur (CHNS), the standard reactants were used: BBOT (2,5-(Bis(5-tert-butyl-2-benzo-oxazol-2-yl) thiophene), methionine, and cysteine. Additionally, vanadium oxide ($V_2O_5$) was added in order to ensure good resolution of the peaks. BBOT and benzoic acid were used to determine the oxygen (O) content. All the samples were dried at 103 ± 2 °C and stored in a desiccator until the analysis and the experiments were performed in triplicate.

Since lignocellulosic biomass are composed of three main chemical components (cellulose, hemicellulose, lignin), a review of its elemental and proximate analyses is shown in Table 1 for comparison proposes.

#### *2.2.2. Surface area BET analysis and porosity characteristics*

The surface area evolution of the samples was evaluated by the adsorption of nitrogen at 77 K in the Micromeritics 3Flex surface characterization analyzer. Prior to analysis, the samples were outgassed at 80 °C until achieving a residual pressure of $10^{-4}$ mmHg, which lasted for different periods of time according to the surface area of each sample. BET surface area, from the isotherms, was calculated using the Brunauer-Emmett-Teller (BET) equation. The relative pressure ($P/P_0$) range that was considered was 0.01 to 0.30 and was assumed to be 0.162 $nm^2$, which is the cross-sectional area for a nitrogen molecule. The total mass of the samples used was enough to achieve a good isotherm plot without mathematical smoothing. The pore size distribution was calculated using the Density Functional Theory (DFT) and the total pore volumes were determined from a single adsorption point at a relative pressure $P/P_0 \geq 0.95$. The experiments were performed in triplicate.

#### *2.2.3. Environmental scanning electron microscopy (ESEM) and scanning electron microscopy with a field emission gun (SEM-FEG)*

Two microscopy analyses were conducted. First, particles (2 mm size), before and after the treatment at 250 °C and 550 °C were evaluated using a FEI Quanta 200 to observe the global changes, under low vacuum, at 0.6 Torr and 12.5 kV. Second, the char residues were recovered from the thermo-gravimetric devices with tungsten and observed, using the Leo 1530

Table 1: Elemental and proximate analyses of the main components of biomasses

| components | | Ref. [a] | elemental analysis (%wt) | | | proximate analysis (%wt) | | |
|---|---|---|---|---|---|---|---|---|
| | | | C | H | O | Ash | VM[b] | FC[c] |
| Cellulose | Micro-crystalline cellulose | [21] | 44.4 | 5.8 | 49.3 | 0 | 94.8 | 5.2 |
| | Sigmacell micro-crystalline cellulose | | 44.5 | 5.6 | 49.5 | 0 | 94.1 | 5.9 |
| | Micro-crystalline cellulose powder | [22] | 39.99 | 5.8 | 54.2 | 0.51 | 98.7 | 0.8 |
| | Pure cellulose | [23] | 42.06 | 6.06 | 46.38 | - | 89.20 | 5.30 |
| Hemicellulose | Xylan from birchwood | [21] | 46.7 | 5.7 | 47.4 | 4.1 | 73.3 | 22.6 |
| | Xylan from beechwood | | 44.3 | 5.4 | 49.9 | 4.8 | 75.3 | 19.9 |
| | Xylan from oat spelts | | 44.8 | 5.6 | 49.5 | 10.1 | 71.1 | 18.8 |
| Lignin | Alkali lignin | [21] | 56.6 | 4.2 | 37.1 | 10 | 49.9 | 40.1 |
| | Lignin from Borregaard | | 65 | 4.9 | 28.7 | 13.5 | 45 | 41.5 |
| | Lignin from Meadwestvaco | | 66.7 | 5.6 | 26.1 | 2.4 | 58.9 | 38.7 |
| | Organic-solved lignin | [22] | 49.53 | 4.39 | 46.07 | 1.71 | 93.8 | 4.5 |
| | Pure Lignin | [23] | 47.65 | 4.30 | 19.60 | 12.35 | 35.74 | 38.81 |
| | Alkali Lignin | [24] | 66.5 | 5.8 | 25.3 | 5.7 | - | - |

[a]Differences between the results presented by each author, are attributed to different extraction methods and the origin of raw material

[b]Volatile matters

[c]Fixed carbon

(SEM-FEG) at 2.00 kV and high vacuum, in order to see the main morphological changes in the cellular wall.

#### *2.2.4. Water vapor sorption properties of untreated (control) and treated samples*

Sorption isotherms and hysteresis were measured using a dynamic vapor sorption apparatus (DVS; Surface Measurement Systems Ltd, London, UK) at a temperature of 25 °C. Detailed information about the apparatus can be found in [25]. All of the samples had similar weights 22.2 ± 0.6 mg and were weighed using a sample pan and a micro-balance, which measured the change in the mass under dry nitrogen. The relative humidity (RH) was increased from 0 to 90% in 10% increments. The RH was raised to the next step when the change in sample mass was below 0.002% $min^{-1}$ and remained so for 10 min. After a constant mass was achieved at 90%, the RH was lowered back to zero in the same configuration as each step. Absolute hysteresis was calculated as the difference between the equilibrium moisture content (EMC) during the desorption ($EMC_{desorption}$) and adsorption ($EMC_{adsorption}$) [26]. The experiments were performed in triplicate.

## 3. Results and discussion

The aim of this study is to analytically evaluate and correlate the structural and morphological changes in the coconut endocarp with the mass loss produced by the thermal treatment by using physicochemical evolution to explain and to predict these changes.

### *3.1. Mass change profile as a function of time*

When biomass is pyrolyzed, different depolymerization and devolatilization reactions take place from the polysaccarides and organic polymers decomposition. Anhydrous mass loss during pyrolysis is a consequence of these decompositions and is depicted in Fig. 2.

We can clearly observe three behaviors, which are related to the three main components degradation. The first behavior occurs during the treatment at 250 °C, with a "*fml*" of about 25%. For this level of temperature, the decomposition of hemicellulose and the release of high-volatility compounds and gases (majorly: $H_2O$, $CO$, $CO_2$ and acid compounds) is expected [27, 28].

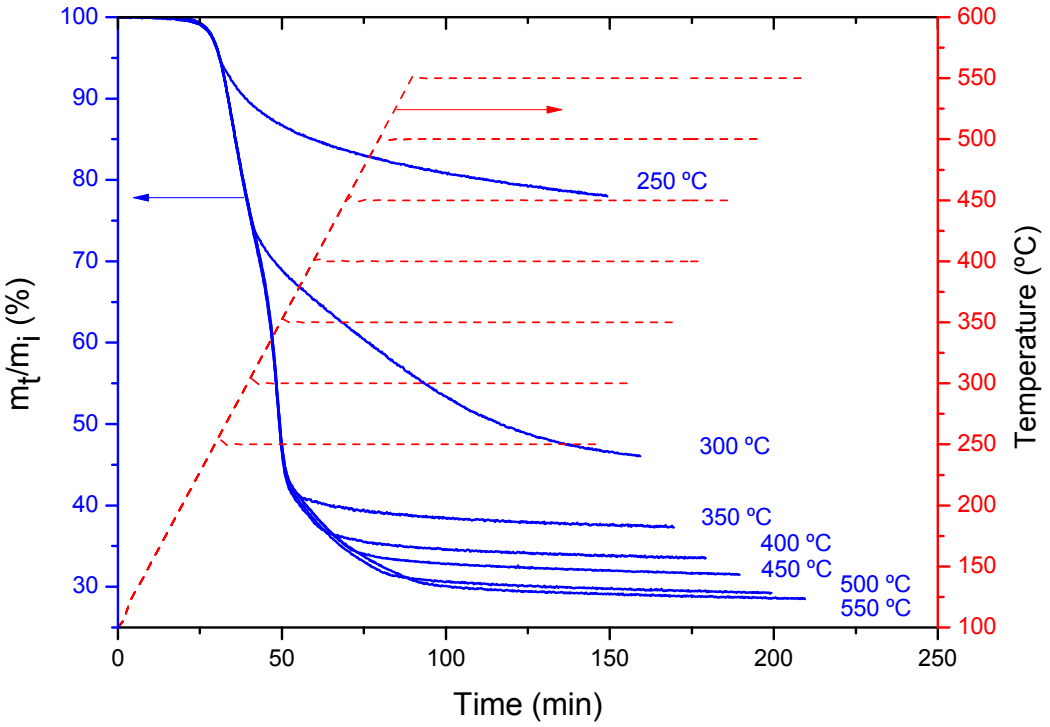


Figure 2: Anhydrous mass loss of coconut endocarp, as a function of time, for each pyrolysis treatment. The red lines indicate the temperature evolution as function of time.

The second behavior is observed in the sample treated at 300 °C. It is mainly the consequence of both hemicellulose and cellulose thermal decomposition. Cellulose degradation is usually explained as a two-step process: an initial reaction step that leads to the formation of "active cellulose", which then undergoes some competitive reactions that produce char plus permanent gases and volatiles (tar) [29, 30, 31]. It is well known that from 300 to 400 °C, cellulose thermal decomposition occurs with a higher decomposition rate that lignin, which decomposes in a wide temperature range (250-500 °C) [32, 33]. The slope in the TG curve, nevertheless exhibits a significant decrease at 350 °C, indicating perhaps, that cellulose has been completely degraded at this temperature level.

The third observed behavior occurs from 350 °C until 550 °C, where the increment in $fml$ was only 19% of the $fml$ observed until 350 °C. This behavior is expected because from 350 °C, the main components in the char residue should be lignin and the degradation solid products derived from

the carbohydrates decomposition. This slow mass decrease was observed in woody biomass [22, 34] as a second stage due the lignin decomposition.

Figure 3 illustrates the DTG curves for untreated and char samples. DTG of coconut endocarp shows two well-defined peaks with a maximum mass-loss rate of 4.84 %wt $min^{-1}$ at 293 °C for the hemicellulose and 9.53 %wt $min^{-1}$ at 365 °C for cellulose decomposition.

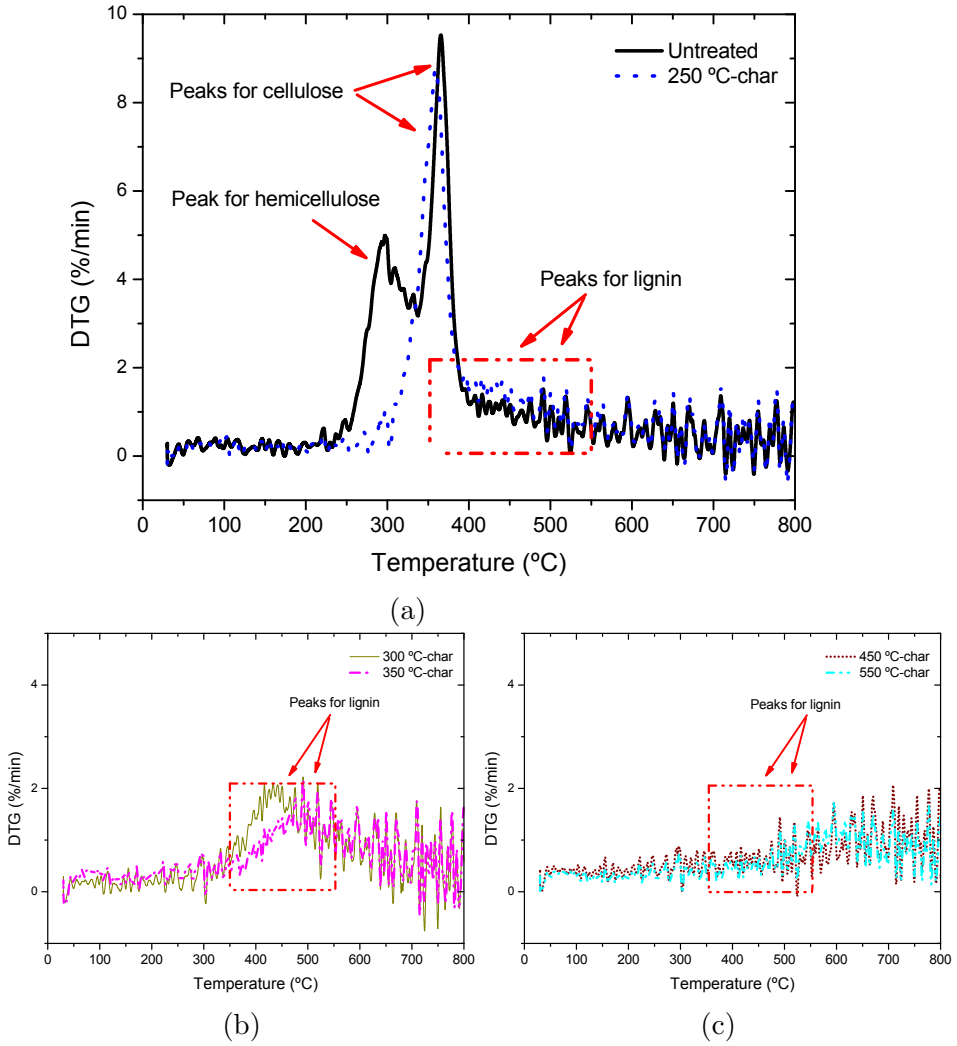


Figure 3: Comparison of DTG curves for (a) untreated and 250 °C-char, (b) 300 °C-char and 350 °C-char, and (c) 450 °C-char and 550 °C-char.

This double-peak was already observed for lignocellulosic biomass with

high lignin contents, such as coconut endocarp (*C. nucifera*) [35, 36]. These authors also explained this double peak by high S/G ratios[1]. Therefore, we expect similar S/G ratio and the presence of p-hydroxybenzoates, proposed as authentic lignin precursors by [37], for our coconut endocarp lignin structure and composition as presented in [35]. However, the S/G ratios for the isolated lignin of coconut endocarp (*C. nucifera*) exhibits different values. These discrepancies could be due the extraction techniques employed [35, 38].

All other peaks, such as hemicellulose and cellulose peaks, were not well-separated in other lignocellulose biomass [32, 39, 40]. A little characteristic shoulder between 350 and 550 °C for lignin which apparently continues until 900 °C according to [34], showed a very slow mass loss that reached 1.40 %wt $min^{-1}$ at 416 °C maximum.

DTG curves for 250 °C-char also depicts the sharp and shoulder peaks for cellulose and lignin, respectively. But the 300 °C-char, exhibited only the characteristic shoulder for lignin on the DTG curve, which indicated that the degradation of cellulose and hemicellulose were completed. This led us to suppose that at most 54 %wt of the coconut endocarp is composed of holocellulose, considering that the lignin decomposed slower than the other components, which is also in accordance with the results presented in [41].

The same shoulder, but at higher temperatures (550 °C), appears for 350 °C-char DTG curve. As lignin is resilient to pyrolysis, its relative content increases with pyrolysis temperature at similar residence time. So, as suggested in [36] higher lignin content can be expected for higher pyrolysis temperatures.

In the chars treated at 450 and 550 °C, this marking shoulder has apparently disappeared.

Mass loss results from numerous competitive reactions and this thermogravimetric curves can give us insight about the reaction mechanisms for the coconut endocarp pyrolysis.

### *3.2. Elemental composition*

Elemental and surface analyses for the untreated and char samples are given in Table 2. Note that sulfur was not detected in any sample.

[1] syringyl- and guaiacyl- lignin units ratio

Table 2: Elemental composition and physical properties for untreated and char samples

| | *fml* | elemental analysis (%wt)[a] | | | | | surface area | total pores volume | micropore volume |
|---|---|---|---|---|---|---|---|---|---|
| | (%wt) | C | H | N | O | S | BET ($m^2/g$) | (cc/g) $\times 10^{-3}$ | (cc/g) $\times 10^{-3}$ |
| Untreated | —— | 51.1 | 5.53 | 0.37 | 42.6 | 0.00 | 0.28 | 0.603 | 0.014 |
| 250 °C-char | 22.0 | 56.9 | 4.95 | 0.40 | 38.6 | 0.00 | 0.30 | 0.322 | 0.079 |
| 300 °C-char | 53.9 | 68.9 | 4.11 | 0.25 | 24.5 | 0.00 | 0.44 | 0.439 | 0.108 |
| 350 °C-char | 62.7 | 71.9 | 3.75 | 0.26 | 21.1 | 0.00 | 0.52 | 0.457 | 0.138 |
| 400 °C-char | 66.5 | 75.1 | 3.34 | 0.27 | 18.1 | 0.00 | 0.57 | 0.520 | 0.175 |
| 450 °C-char | 68.5 | 78.2 | 3.02 | 0.28 | 13.6 | 0.00 | 5.95 | 2.56 | 2.06 |
| 500 °C-char | 70.7 | 82.1 | 2.78 | 0.31 | 9.10 | 0.00 | 108 | 45.7 | 42.3 |
| 550 °C-char | 71.5 | 85.7 | 2.55 | 0.59 | 6.08 | 0.00 | 216 | 89.1 | 84.2 |

[a]For an analyzer detection limit of 0.01% (100 ppm).

Coconut endocarp has a high lignin composition with amounts of carbon (C) higher than 50% and oxygen (O) lower than 43%, in comparison to values reported in Table 1. These results are expected since the coconut endocarp has in average a high lignin content of approximately 35% and hollocelulose content of approximately 53% [1, 41].

Another important observation is that the sum (C + H + N + O) is not equal to 100% from 300 °C-char. This is due to char fraction contains inorganic materials (ash) and its proportion increases with the pyrolysis temperature [42, 43].

The most important thermochemical reactions can be visualized from the van Krevelen diagram (Fig. 4a). Overall, dehydration and decarboxylation reactions, led coconut endocarp to become more lignin-like, even from the first treatment at 250 °C.

Notable oxygen reduction from the initial oxygen content occurs for the sample treated at 300 °C ($\approx$ 24 %), which is expected from the hemicellulose and cellulose decomposition and the devolatilization of low molecular mass products at this temperature.

Considering the oxygen reduction, the low sulfur content and the lignin-like characteristic of char obtained at 250 °C and 300 °C, an interesting output could be the production of high-quality bio-oil for power generation or to produce phenolic-based chemicals.

The slow lignin decomposition explains the low additional oxygen reduction (about 6%) of the samples treated at 400 °C compared with those treated at 300 °C. There is an increase in the mass-loss rate from 400 until 550 °C, in accordance with the DTG curves (Fig. 3) and hence it observed a small increment in oxygen reduction (9%) was observed between the samples treated at 400 and 500 °C.

For the higher thermal treatment of 550 °C, 85.7% of the initial oxygen content has been removed with just 71% of $fml$. It is not trivial to predict the chemical structure of the 6% of oxygen that remains, which should be highly aromatic considering its carbon enrichment. More explanations about the chemical structure of carbonized charcoal can be found in [9].

Charcoal could be used as a reductant, in the production of chemicals, refining of metals, production of activated carbon or just as domestic cooking and heating [44]. The quality of the charcoals depends on the end use. The yields of charcoal obtained in our standard experiment seem promising because the treatment is almost uniform and leads to optimum yields [45, 46].

The van Krevelen diagram demonstrates the energy intensification with

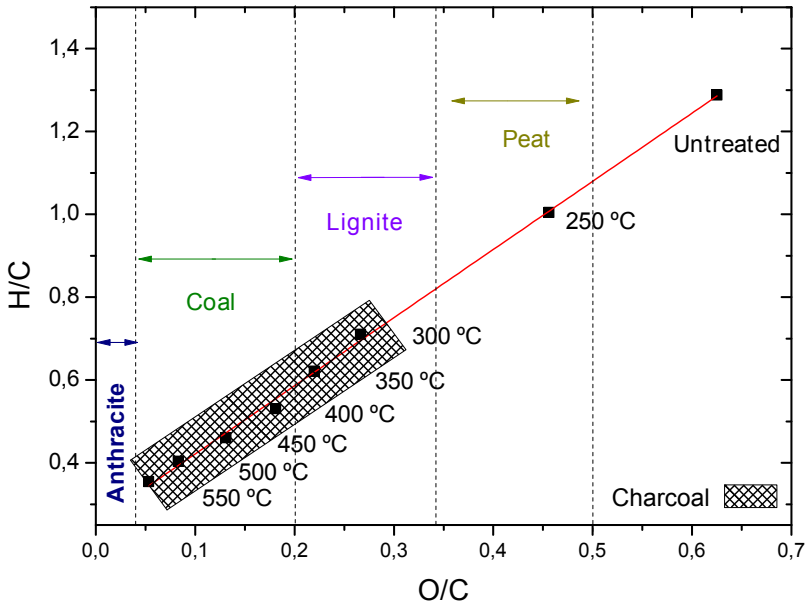


(a)

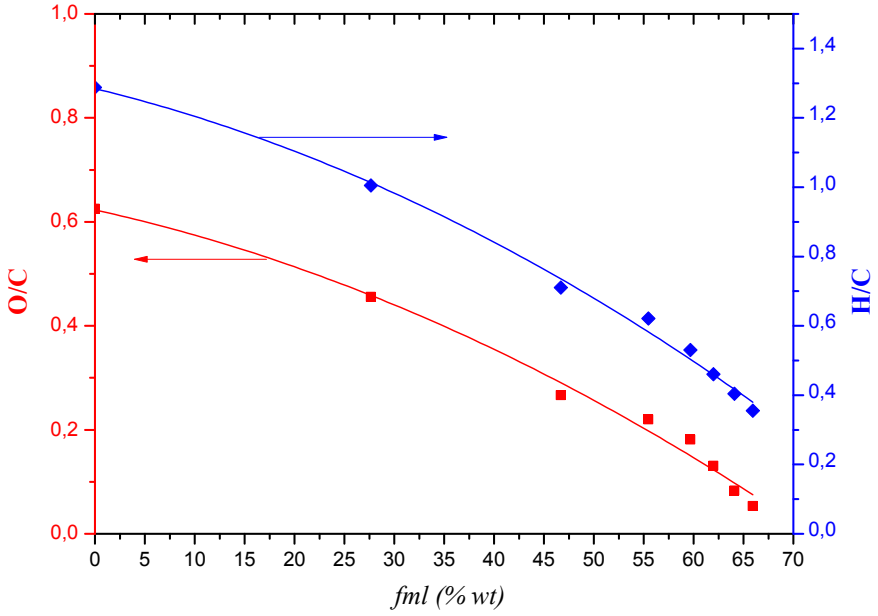


(b)

Figure 4: (a) van Krevelen plot. (b) O/C and H/C ratios as function of the $fml$.

a linear correlation, H/C $\approx$ 1.64 (O/C) + 0.26 ($R^2$ = 0.999), see Fig. 4a. Elementary composition resembles a peat for the treatment at 250 °C and from 300 °C it goes from characteristic charcoal towards anthracite at the higher temperature [47, 48].

Furthermore, Fig. 4b shows a decrease of O/C and H/C ratios as a function of $fml$. A good polynomial approximation can be found for both ratios: O/C $\approx 0.62 - 4 \times 10^{-3}(fml) - 6.18 \times 10^{-5}(fml)^2$ with $R^2 = 0.986$ and H/C $\approx 1.28 - 7 \times 10^{-3}(fml) - 1.02 \times 10^{-4}(fml)^2$ with $R^2 = 0.993$. These results show potential feasible application of the charcoals for electric power generation, for example, via biomass integrated gasification gas turbine (BIG/GT) technologies [44, 49], that could compete with fossil fuels, also fewer emission and gas cleaning problems (from its lower nitrogen, sulfur and ash contents) are expected.

Physicochemical properties such oxidation stability and moisture sorption capacity can be predicted from the H/C and O/C ratios. Indeed, a considerable reduction in the number of polar sites from the O/C ratio reduction is expected and therefore a lower hygroscopicity in such chars. In [50], it was proposed for a first time a parameter "Z", ($Z = 2(O/C) - (H/C)$) to computed the average carbon oxidation state. The Z values computed as in [50], displays negative values for all chars here, in agreement with a reduced states of carbon (lignin is most reduced), which has a pronounced effect on its chemical reactivity.

### *3.3. Surface area and pore size analysis*

Table 2 also displays the specific BET surface area and pore volume for the untreated and char samples. The untreated and char, obtained up to 400 °C, had very low surface areas, lower than 0.6 $m^2/g$, and a total pore volume lower than $0.52 \times 10^{-3}$ cc/g. This behavior is explained by considering the high lignin content in the coconut endocarp, which could obstruct the pores since alkali lignin pyrolysis displayed a melting even at low temperatures of 250 °C [24, 51], resulting in low surface area until 350 °C, where the primary devolatilization process is less pronounced.

The low surface area of 400 °C-char could be attributed to coke formation as a consequence of tar cracking by the secondary heterogeneously reactions [52, 53], which may occur even in the pores of the particles [17]. Others authors [9] also justify the low surface area for carbonized charcoal of melt carbons (at 950 °C) as consequence of this liquid phase ocurring during pyrolysis. The 450 °C-char exhibits an exponential increase in the surface area,

reaching a value of 216 $m^2/g$ and total pore volume of 0.089 cc/g for the higher thermal treatment of 550 °C, which represents an increment of more than a thousand times the untreated sample.

Coconut endocarp presented typical adsorption isotherm type II (Fig. 5a), in accordance with the Brunauer classifications. In addition, char obtained until 400 °C showed the same type II isotherms, but less pronounced than those that were left untreated. From 450 °C, the adsorption isotherms change from Type II to Type I, characteristic of microporous materials, with at least 80% of total pore volume adsorbed ($\approx 2.56 \times 10^{-3} cc/g$) corresponding to microporous volume ($\approx 2.06 \times 10^{-3} cc/g$).

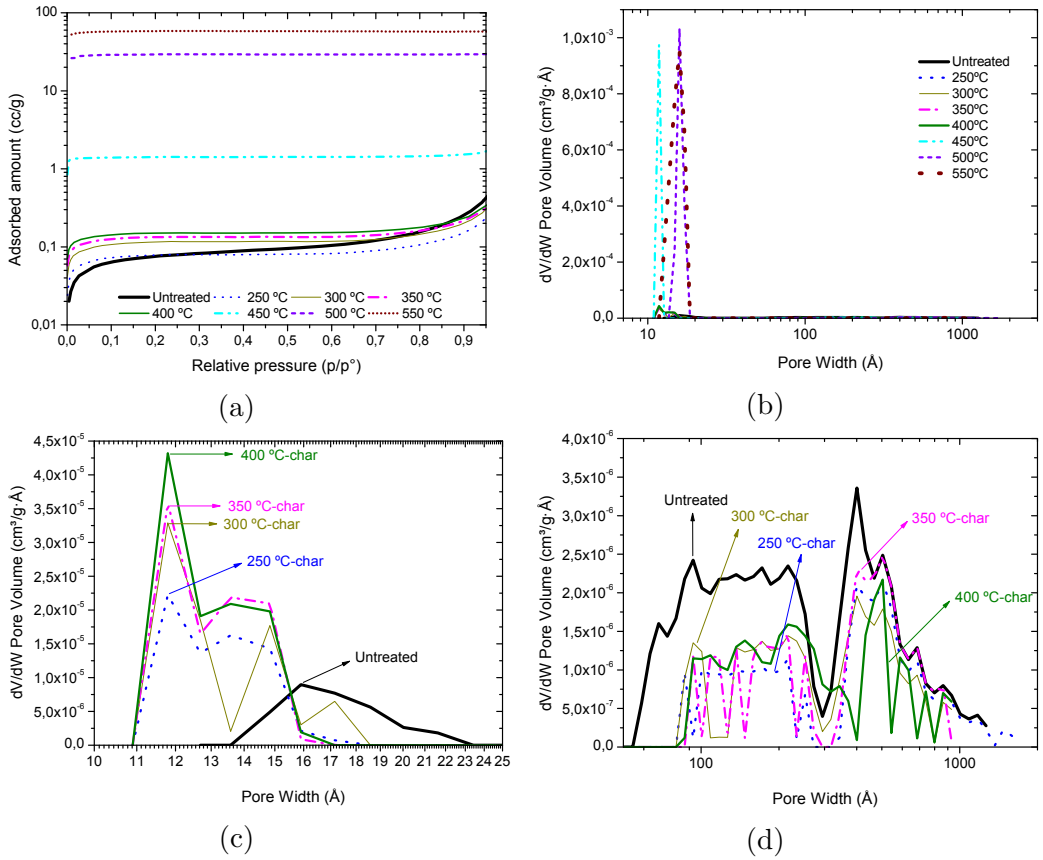


Figure 5: (a) Adsorption isotherms for the untreated and treated samples. (b) Pore size distribution (PSD) by Density functional theory (DFT) for untreated and treated samples (Below). (c) Amplification of PSD for the untreated and chars treated until 400 °C, from 10 to 15 Å, and (d) from 25 until 200 Å.

Furthermore, the pore size distribution (PSD) in the chars, Fig. 5b, shows that the exponential increment in the surface area is a consequence of the micropore development, with a pore width between 10 and 20 Å. To put this value in perspective, the diameter of the glucose molecule is 80 Å. Considering the microfibrils are composed of many chain of cellulose, the diameter of the microfibrils is more than 500 Å.

A zoom of the PSD for untreated and char samples until 400 °C, is presented in Fig. 5c and 5d. Although these samples are not microporous, the small peaks detected between 10-25 Å of the pore width, match with the size of micro-voids naturally presented in the cell walls of cellulose samples [54], which apparently suffers a little contraction with thermal treatment. In addition, peaks were detected in the range corresponding to mesoporous and macroporous materials (Fig. 5d), with reduced intensity as a consequence of the thermal treatment until reaching 400 °C. These peaks, detected between 100-2000 Å of pore width, could represent simple pores, presented naturally in the scleroids cell walls and as will be seen later in the results of the SEM/FEG micrographs.

From its microporous structure, surface area and carbon content, the 500 °C-char and 550 °C-char are proposed as a raw material for activated carbon or syngas production from the gasification process, due to its expected more uniform gas transfer, which should maintain the gasification reactivity with elapsed time [55].

Finally, these results clearly show that the coconut endocarp undergoes chemical changes as a consequence of the primary decomposition, but not major changes in the porous structure until 450 °C.

### *3.4. ESEM and SEM-FEG visualization*

Morphological changes of a single particle, as a consequence of the lower (250 °C) and higher (550 °C) temperature of treatment, are displayed in Figure 6. Simple pores, of about 1 $\mu m$ of pore width, naturally present in cell walls, are observed in the untreated samples. It is possible to observe that the initial physical shape of the cell wall remains, even for the more intense treatments at 550 °C (Fig. 6d), but with a significant contraction in the structure of the sample, which is apparently submerged in a molten fibrous mass.

Figure 7 illustrate the SEM/FEG micrographs for untreated and char samples, obtained at 250 °C, 350 °C, and 550 °C. Apparently, an initial softening in the chars treated at 250 °C and 350 °C, is observed (Fig. 7b and

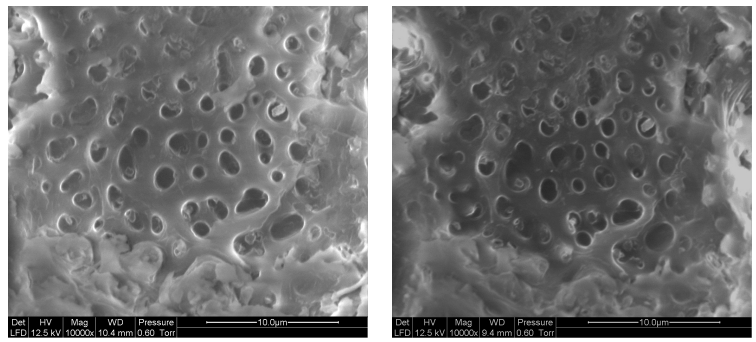

(a) Untreated (b) $ml_{250°C} = 22.0\%$

(c) Untreated (d) $ml_{550°C} = 71.5\%$

Figure 6: Morphological and structural changes over a single particle for the lower (a-b) and higher (c-d) temperature of treatment.

7c). As the intensity of treatment increases, the 550 °C-char appears to melt as displayed in the Figure 7d. These results are consistent with observations in lignin chars obtained in the same range of temperatures [24] and allow us to suppose that the low surface areas in the chars until 400 °C, could be a consequence of this softening.

Other SEM/FEG visualizations, not displayed here, allowed us to see the fibrous structure of the cell walls, which are composed of sclereid cells [2, 15]. The sclereids appear as columnar cells, with about 20 $\mu m$ of diameter and variable depth. The longest dimension of the fiber bundle was difficult to define, but it was possible to observe that the fiber was longer than 50 $\mu m$, with a thickness higher than 500 Å, which is in agreement with the microfibrils diameter.

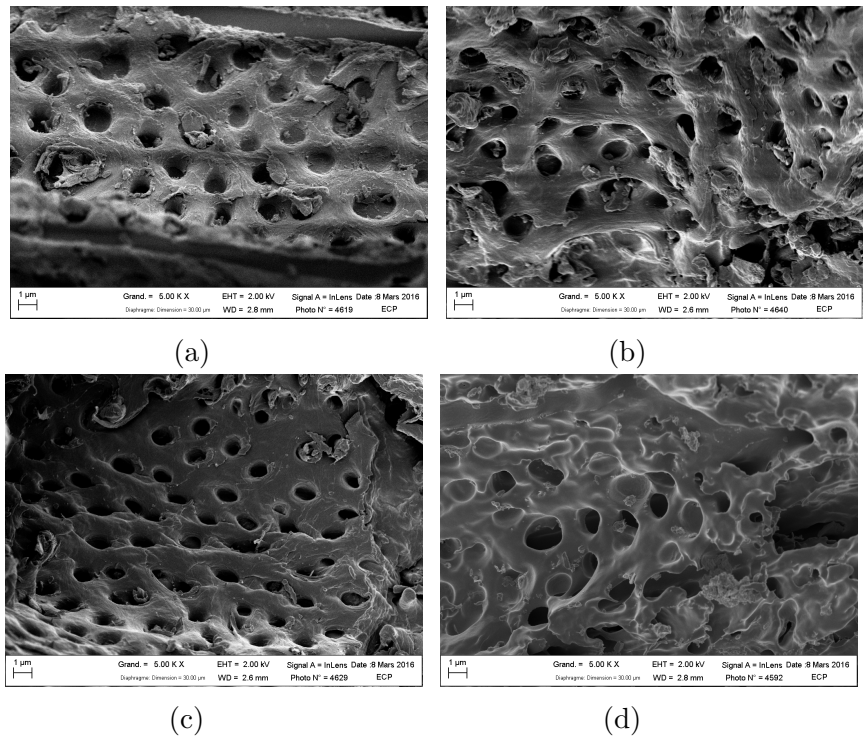


Figure 7: SEM/FEG micrographs of (a) coconut endocarp and its chars obtaining at (b) 250 °C, (c) 350 °C and (d) 550 °C.

### *3.5. Dynamic vapor sorption isotherms*

An important factor in the moisture sorption properties of polymers is the hydroxyl groups (OH) accessibility, termed as sorption sites, because these OH-groups have strong hydrogen bond-interaction with water molecules.

Although cellulose has many OH-groups, only 33% of these are accessible, whereas the surface of the microfibrils are considered sorption sites [56]. Estimation of these sorption sites in wood, based on the molecular mass of its main components, had a very high water-accessible OH concentration for Xylan and Glucomannan [56] in comparison with cellulose and lignin concentrations.

Figure 8 shows the sorption isotherms for the coconut endocarp and chars samples. It should be noted that the EMC in the coconut endocarp was lower than the typical values presented for wood samples [11, 12, 26, 57]. The coconut endocarp also contains about 53% of holocellulose [41], of which less than 22% is hemicellulose from the $fml$ and DTG of the 250 °C-char. These

results are presented in Table 2 and Fig. 3. Its composition, together with the random distribution of its highly lignified sclereids cells [2], is responsible for its natural, more hydrophobic character, which explain its low values of EMC. In all cases, charring resulted in a decrease of the average EMC.

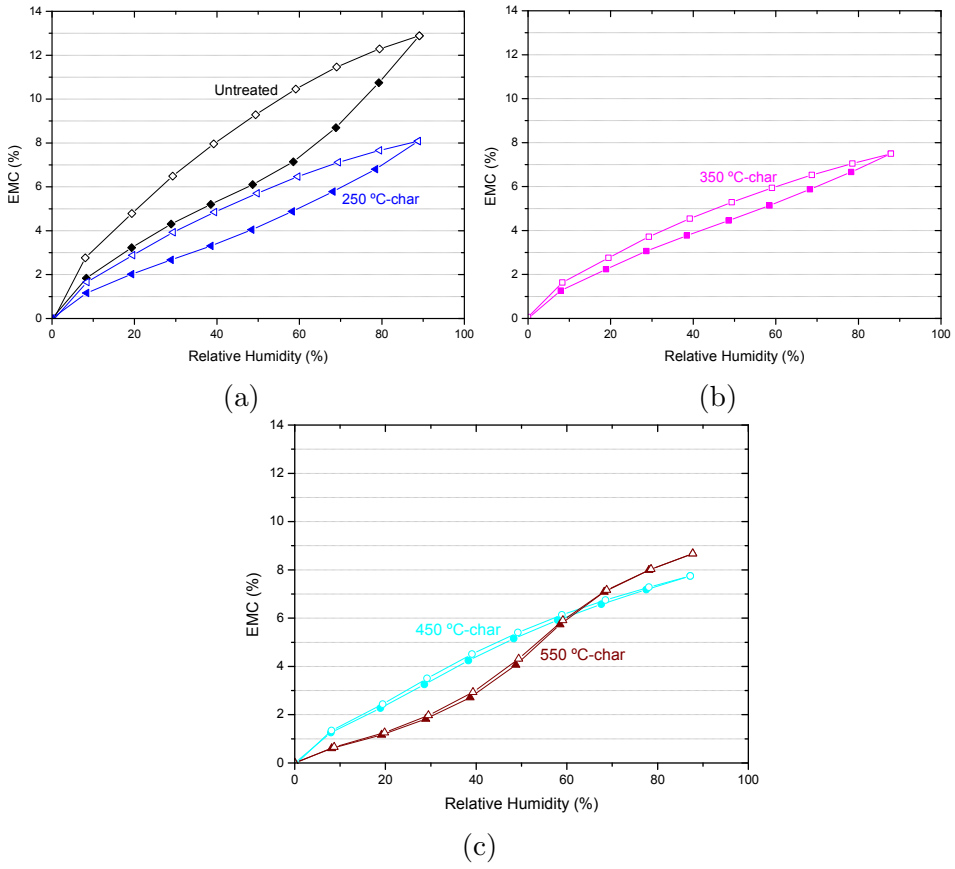


Figure 8: Dynamic vapor sorption isotherms for: (a) untreated and 250 °C-char, (b) 350 °C-char, (c) 450 °C-char and 550 °C-char.

It is also possible to observe the changes in the isotherm shape during pyrolysis. Typical sigmoidal type II curves for cellulosic materials are presented. Both the untreated sample (Fig. 8a) and 250 °C-char exhibit this sigmoid shape as a result of their cellulose content and based on the fact that hemicellulose was decomposed at this temperature (Fig. 3). The isotherms going through a combination of type I and type II for 350 °C-char (Fig. 8b), because no more cellulose remains and, as expected, there is a higher lignin

fraction (Fig. 3) and do not show a microporous structure, unlike the 450 °C-char which exhibits the characteristic type I isotherm (Fig. 8c).

The pronounced curve type V for the char obtained at 550 °C (Fig. 8c) is explained by its higher carbon content of about 86%. The charcoal has a particular water adsorption behavior, which was already explained by [58]. This behavior is considered an initial weak uni-molecular attraction between the carbon-water molecules at low RH values. As soon as the water molecules become adsorbed and the RH increases, the next strongest interaction between water molecules happens more easily within the micro-voids until they are filled.

At relative humidity values higher than 60% RH, the EMC for the 550 °C-char increases with respect to the 450 °C-char; this is a consequence of its high microvoids number (Fig. 8c). The micro-porous volume is indicative of the micro-void quantities present in the charcoal structure which, for the 550 °C-char, is forty times more than that for 450 °C-char. Then, the isotherm type V would be in effect a type I isotherm, considering its microporous structure, which matches with our previous results of $N_2$ type I adsorption isotherms.

Similar sorption behaviors were obtained for torrefied and charcoal wood up to 450 °C [12, 11, 59], but with different holding times at each peak temperature.

Figure 9 shows that absolute hysteresis decreases as the pyrolysis intensity increases; this is a consequence of overall decreases on the hygroscopicity. The higher value of 3.32% was found in coconut endocarp at 60% RH.

The hysteresis ratio agreed with the results obtained in the mild thermal treatment of wood [57]. The small increases in hysteresis ratio is explained by the authors as a product of the stiffness increases with the higher times of treatment.

The pore geometry has influence over the hysteresis, thus capillary condensation in mesopores with narrow necks and wide bodies could occur, in the multilayer adsorption range or in micropores with narrow slip-like pores materials [60]. A hysteresis model has been proposed in [13] as result of different states (expansion and collapse of nanoporous in the cell-walls matrix) of the material in which the adsorption and desorption process will take place.

The microcapillaries or microvoids measure a diameter of 2-10 nm in wood samples [54]. The pore size distribution shown in Fig. 5c, for the untreated and chars until 400 °C, match this range. The desorption process takes place

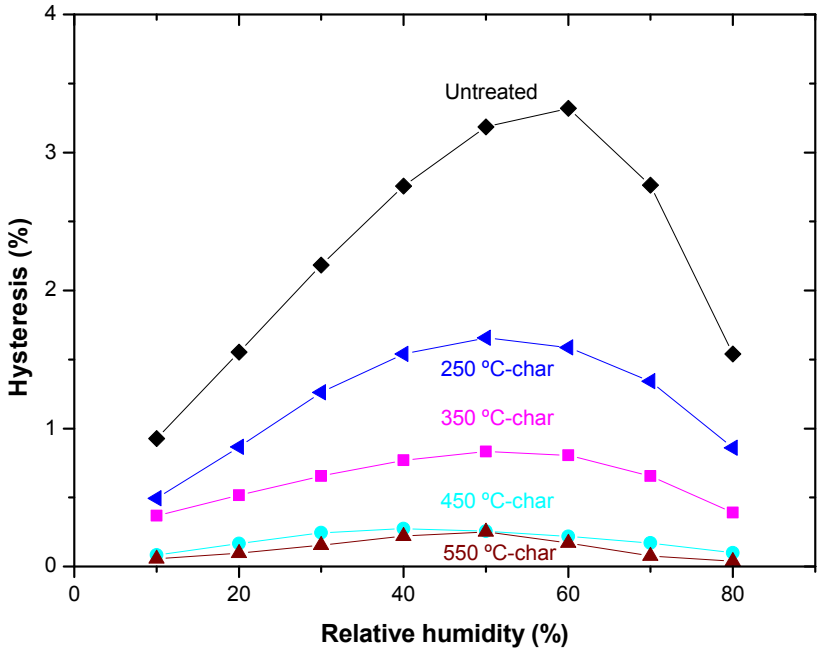


Figure 9: Absolute hysteresis of coconut endocarp and its chars at 0-90 % of RH.

in a swelling matrix, resulting from the hydrogen-bonds and hemicellulose, within the microcapillaries. A pore collapse could occur during the desorption process for an untreated sample.

Similarly, hysteresis in 250 °C-char and 350 °C-char is explained by the water retention inside the collapse matrix, which will be less due at the lower sorption sites in cellulose. The lignin content could present a higher deformation facility to accomodate water, so, we expect that in the desorption process, its deformation capacity could avoid the matrix collapse, thus reducing the hysteresis.

Char obtained at 450 °C and 550 °C present with negligible hysteresis. Both, have significant microporosity, which was confirmed by the exponential increases in the surface area BET and the pore size distribution (Table 2 and Fig. 5b). Microporous charcoals from different feedstock show hysteresis [9] for nitrogen adsorption, which was explained to be the result of pore shape, like narrow slit-shaped pores, that impede the diffusion of adsorbate [61]. Also, microporous activated carbon shown a significantly high hysteresis as consequence of its functional groups, which increases the interaction with the

water molecules [62].

Recently, the loss of hysteresis for charcoal of wood was explained as consequence of inaccessible internal porosity or negligible micropore formation which consequently increases in stiffness that avoids the micropore creation/destruction mechanism [12]. We wish to suggest an alternative explanation. Given sufficient time, water will enter pores smaller than 4-5 Å with dimensions comparable to that of the water molecules [63]. The lack of hysteresis in these two charcoals is most likely related to diffusional aspects. For example, as a consequence of the geometrical pore shape that is more suitable to the mechanism of egress of water molecules; and the poor interaction between the water molecules and the substrate, which facilitates its release during the desorption process.

## 4. Conclusion

Prior work emphasized the enormous potential of coconut endocarp as raw material to produce biofuel, charcoal or activated carbon. However, these studies were not focused on its physicochemical evolution along the thermal decomposition. In the present work, different analytical methods were used to assess the product alterations due to pyrolysis: elemental analysis, surface area and pore size analyses, ESEM and SEM/FEG observation and dynamic vapor sorption determination.

At low temperature, the main effect is on the oxygen content, with a gradual shift from native biomass to charcoal, which is preferable as solid fuel or as feedstock to high-quality bio-oil. DTG curves indicate that the product becomes lignin-like from a thermal treatment at 300 °C. At higher temperature, this trend continues, shifting towards fixed carbon and above 450 °C, the chars acquire microporous materials characteristics with an exponential increase of the specific surface and low hygroscopicity values. This allows such treated products to be considered as raw materials in a gasification process to produce syngas or activated carbon.

In addition, we proposed expressions for O/C and H/C ratios as a function of the mass loss that can be used for prediction purposes. To our knowledge, this is the first investigation of the sorption properties, BET surface area and morphology evolution along the thermal decomposition of coconut endocarp —*Acrocomia aculeata* —.

Our results provide sufficient evidence for the long-term application of this feedstock and its chars as solid fuel or raw material in the gasification

process. However, the combustion characteristics and gasification conditions still need be tested.

## Acknowledgment

The authors thank Nathalie Ruscassier for assistance with SEM/FEG, Mathilde Charters and Gonalo de Bastos Monteiro for help with surface area BET analysis. S. Duarte thanks the support of CONACYT under grant Code Project 14-INV-087. Financial supports from Grand Reims, the Marne department and the Grand Est region are gratefully acknowledged.

## References

[1] A. B. Evaristo, J. A. S. Grossi, A. d. C. O. Carneiro, L. D. Pimentel, S. Y. Motoike, K. N. Kuki, Actual and putative potentials of macauba palm as feedstock for solid biofuel production from residues, Biomass and Bioenergy 85 (2016) 18–24.

[2] S. B. Reis, M. O. Mercadante-Simes, L. M. Ribeiro, Pericarp development in the macaw palm acrocomia aculeata (arecaceae), Rodrigusia 63 (2012) 541–549.

[3] M. Plath, C. Moser, R. Bailis, P. Brandt, H. Hirsch, A.-M. Klein, D. Walmsley, H. von Wehrden, A novel bioenergy feedstock in Latin America? Cultivation potential of Acrocomia aculeata under current and future climate conditions, Biomass and Bioenergy 91 (2016) 186 – 195.

[4] G. Ciconini, S. Favaro, R. Roscoe, C. Miranda, C. Tapeti, M. Miyahira, L. Bearari, F. Galvani, A. Borsato, L. Colnago, M. Naka, Biometry and oil contents of Acrocomia aculeata fruits from the Cerrados and Pantanal biomes in Mato Grosso do Sul, Brazil, Industrial Crops and Products 45 (2013) 208 – 214.

[5] I. Gauto, R. E. Spichiger, F. W. Stauffer, Diversity, distribution and conservation status assessment of Paraguayan palms (Arecaceae), Biodiversity and Conservation 20 (2011) 2705–2728.

[6] J. Poetsch, D. Haupenthal, I. Lewandowski, D. Oberländer, T. Hilger, Acrocomia aculeataa sustainable oil crop, Rural 21 (2012) 41–44.

[7] S. J. Duarte, J. Lin, D. Alviso, J. C. Rolón, Effect of Temperature and Particle Size on the Yield of Bio-oil, Produced from Conventional Coconut Core Pyrolysis, International Journal of Chemical Engineering and Applications 7 (2016) 102–108.

[8] K. Mochidzuki, F. Soutric, K. Tadokoro, M. J. Antal, M. Tóth, B. Zelei, G. Várhegyi, Electrical and physical properties of carbonized charcoals, Industrial & Engineering Chemistry Research 42 (2003) 5140–5151.

[9] J. Bourke, M. Manley-Harris, C. Fushimi, K. Dowaki, T. Nunoura, M. J. Antal, Do all carbonized charcoals have the same chemical structure? 2. A model of the chemical structure of carbonized charcoal, Industrial & Engineering Chemistry Research 46 (2007) 5954–5967.

[10] M. Keiluweit, P. S. Nico, M. G. Johnson, M. Kleber, Dynamic molecular structure of plant biomass-derived black carbon (biochar), Environmental Science & Technology 44 (2010) 1247–1253.

[11] C.-M. Popescu, C. A. Hill, R. Anthony, G. Ormondroyd, S. Curling, Equilibrium and dynamic vapour water sorption properties of biochar derived from apple wood, Polymer Degradation and Stability 111 (2015) 263–268.

[12] M. Kymäläinen, L. Rautkari, C. A. S. Hill, Sorption behaviour of torrefied wood and charcoal determined by dynamic vapour sorption, Journal of Materials Science 50 (2015) 7673–7680.

[13] C. A. S. Hill, A. Norton, G. Newman, The water vapor sorption behavior of natural fibers, Journal of Applied Polymer Science 112 (2009) 1524–1537.

[14] W. Willems, The water vapor sorption mechanism and its hysteresis in wood: the water/void mixture postulate, Wood Science and Technology 48 (2014) 499–518.

[15] H. C. Mazzottini-dos Santos, L. M. Ribeiro, M. O. Mercadante-Simões, B. F. Sant'Anna-Santos, Ontogenesis of the pseudomonomerous fruits of Acrocomia aculeata (Arecaceae): a new approach to the development of pyrenarium fruits, Trees 29 (2015) 199–214.

[16] T. J. Hilbers, Z. Wang, B. Pecha, R. J. Westerhof, S. R. Kersten, M. R. Pelaez-Samaniego, M. Garcia-Perez, Cellulose-lignin interactions during slow and fast pyrolysis, Journal of Analytical and Applied Pyrolysis 114 (2015) 197 – 207.

[17] C. D. Blasi, Modeling chemical and physical processes of wood and biomass pyrolysis, Progress in Energy and Combustion Science 34 (2008) 47 – 90.

[18] C. D. Blasi, Numerical simulation of cellulose pyrolysis, Biomass and Bioenergy 7 (1994) 87 – 98.

[19] E. Bohn, Tablero de comando para la promoción de los biocombustibles en Paraguay, Technical Report, Naciones Unidas Comisión Económica para América Latina y el Caribe (CEPAL), 2009.

[20] G. Almeida, J. Brito, P. Perré, Alterations in energy properties of eucalyptus wood and bark subjected to torrefaction: The potential of mass loss as a synthetic indicator, Bioresource Technology 101 (2010) 9778 – 9784.

[21] C. Couhert, J.-M. Commandre, S. Salvador, Is it possible to predict gas yields of any biomass after rapid pyrolysis at high temperature from its composition in cellulose, hemicellulose and lignin?, Fuel 88 (2009) 408–417.

[22] A. Gani, I. Naruse, Effect of cellulose and lignin content on pyrolysis and combustion characteristics for several types of biomass, Renewable Energy 32 (2007) 649–661.

[23] D. Lv, M. Xu, X. Liu, Z. Zhan, Z. Li, H. Yao, Effect of cellulose, lignin, alkali and alkaline earth metallic species on biomass pyrolysis and gasification, Fuel Processing Technology 91 (2010) 903–909.

[24] R. K. Sharma, J. B. Wooten, V. L. Baliga, X. Lin, W. G. Chan, M. R. Hajaligol, Characterization of chars from pyrolysis of lignin, Fuel 83 (2004) 1469–1482.

[25] C. A. S. Hill, A. J. Norton, G. Newman, The water vapour sorption properties of sitka spruce determined using a dynamic vapour sorption apparatus, Wood Science and Technology 44 (2010) 497–514.

[26] C. A. S. Hill, J. Ramsay, B. Keating, K. Laine, L. Rautkari, M. Hughes, B. Constant, The water vapour sorption properties of thermally modified and densified wood, Journal of Materials Science 47 (2012) 3191–3197.

[27] J. Wannapeera, B. Fungtammasan, N. Worasuwannarak, Effects of temperature and holding time during torrefaction on the pyrolysis behaviors of woody biomass, Journal of Analytical and Applied Pyrolysis 92 (2011) 99 – 105.

[28] M. J. Prins, K. J. Ptasinski, F. J. Janssen, Torrefaction of wood: Part 2. analysis of products, Journal of Analytical and Applied Pyrolysis 77 (2006) 35 – 40.

[29] A. G. Bradbury, Y. Sakai, F. Shafizadeh, A kinetic model for pyrolysis of cellulose, Journal of Applied Polymer Science 23 (1979) 3271–3280.

[30] J. Piskorz, D. S. A. Radlein, D. S. Scott, S. Czernik, Pretreatment of wood and cellulose for production of sugars by fast pyrolysis, Journal of Analytical and Applied Pyrolysis 16 (1989) 127–142.

[31] J. L. Banyasz, S. Li, J. L. Lyons-Hart, K. H. Shafer, Cellulose pyrolysis: the kinetics of hydroxyacetaldehyde evolution, Journal of Analytical and Applied Pyrolysis 57 (2001) 223–248.

[32] E. Jakab, Chapter 3 - Analytical Techniques as a Tool to Understand the Reaction Mechanism, in: A. Pandey, T. Bhaskar, M. Stcker, R. K. Sukumaran (Eds.), Recent Advances in Thermo-Chemical Conversion of Biomass, Elsevier, Boston, 2015, pp. 75 – 108.

[33] P. Lv, G. Almeida, P. Perré, TGA-FTIR Analysis of Torrefaction of Lignocellulosic Components (cellulose, xylan, lignin) in Isothermal Conditions over a Wide Range of Time Durations, BioResources 10 (2015) 4239–4251.

[34] H. Yang, R. Yan, H. Chen, D. H. Lee, C. Zheng, Characteristics of hemicellulose, cellulose and lignin pyrolysis, Fuel 86 (2007) 1781–1788.

[35] A. E. Harman-Ware, M. Crocker, R. B. Pace, A. Placido, S. Morton III, S. DeBolt, Characterization of endocarp biomass and extracted lignin using pyrolysis and spectroscopic methods, BioEnergy Research 8 (2015) 350–368.

[36] V. Mendu, A. E. Harman-Ware, M. Crocker, J. Jae, J. Stork, S. Morton, A. Placido, G. Huber, S. DeBolt, Identification and thermochemical analysis of high-lignin feedstocks for biofuel and biochemical production, Biotechnology for biofuels 4 (2011) 43.

[37] J. Ralph, Hydroxycinnamates in lignification, Phytochemistry Reviews 9 (2010) 65–83.

[38] J. Rencoret, J. Ralph, G. Marques, A. Gutierrez, A. T. Martínez, J. C. del Rio, Structural characterization of lignin isolated from coconut (cocos nucifera) coir fibers, Journal of agricultural and food chemistry 61 (2013) 2434–2445.

[39] P. H. G. Cademartori, P. S. d. Santos, L. Serrano, J. Labidi, D. A. Gatto, Effect of thermal treatment on physicochemical properties of gympie messmate wood, Industrial Crops and Products 45 (2013) 360–366.

[40] T. Sonobe, N. Worasuwannarak, Kinetic analyses of biomass pyrolysis using the distributed activation energy model, Fuel 87 (2008) 414–421.

[41] J. d. C. Silva, L. E. G. Barrichelo, J. O. Brito, Endocarpos de babaçu e de macaúba comparados à madeira de eucalyptus grandis para a produção de carvão vegetal, Ipef 34 (1986) 31–34.

[42] M. I. Al-Wabel, A. Al-Omran, A. H. El-Naggar, M. Nadeem, A. R. Usman, Pyrolysis temperature induced changes in characteristics and chemical composition of biochar produced from conocarpus wastes, Bioresource technology 131 (2013) 374–379.

[43] S. Yaman, Pyrolysis of biomass to produce fuels and chemical feedstocks, Energy conversion and management 45 (2004) 651–671.

[44] M. J. Antal, E. Croiset, X. Dai, C. DeAlmeida, W. S.-L. Mok, N. Norberg, J.-R. Richard, M. Al Majthoub, High-yield biomass charcoal, Energy & Fuels 10 (1996) 652–658.

[45] L. Wang, M. Trninic, Ø. Skreiberg, M. Gronli, R. Considine, M. J. Antal Jr, Is elevated pressure required to achieve a high fixed-carbon yield of charcoal from biomass? part 1: Round-robin results for three different corncob materials, Energy & Fuels 25 (2011) 3251–3265.

[46] L. Wang, Ø. Skreiberg, M. Gronli, G. P. Specht, M. J. Antal Jr, Is elevated pressure required to achieve a high fixed-carbon yield of charcoal from biomass? part 2: The importance of particle size, Energy & Fuels 27 (2013) 2146–2156.

[47] J. J. Chew, V. Doshi, Recent advances in biomass pretreatment–torrefaction fundamentals and technology, Renewable and Sustainable Energy Reviews 15 (2011) 4212–4222.

[48] S. Cavagnol, J. F. Roesler, E. Sanz, W. Nastoll, P. Lu, P. Perré, Exothermicity in wood torrefaction and its impact on product mass yields: From micro to pilot scale, The Canadian Journal of Chemical Engineering 93 (2015) 331–339.

[49] P. McKendry, Energy production from biomass (part 2): conversion technologies, Bioresource technology 83 (2002) 47–54.

[50] W. Willems, C. Mai, H. Militz, Thermal wood modification chemistry analysed using van krevelen's representation, International Wood Products Journal 4 (2013) 166–171.

[51] V. Baliga, R. Sharma, D. Miser, T. McGrath, M. Hajaligol, Physical characterization of pyrolyzed tobacco and tobacco components, Journal of Analytical and Applied Pyrolysis 66 (2003) 191 – 215.

[52] Y. Zhang, S. Kajitani, M. Ashizawa, K. Miura, Peculiarities of rapid pyrolysis of biomass covering medium-and high-temperature ranges, Energy & fuels 20 (2006) 2705–2712.

[53] D. Dayton, A review of the literature on catalytic biomass tar destruction, US DOE NREL Report Golden, CO (2002) 510–32815.

[54] C. A. Hill, A. N. Papadopoulos, A review of methods used to determine the size of the cell wall microvoids of wood, Journal-Institute of Wood Science 15 (2001) 337–345.

[55] Q. Xu, S. Pang, T. Levi, Reaction kinetics and producer gas compositions of steam gasification of coal and biomass blend chars, part 1: Experimental investigation, Chemical engineering science 66 (2011) 2141–2148.

[56] E. T. Engelund, L. G. Thygesen, S. Svensson, C. A. S. Hill, A critical discussion of the physics of woodwater interactions, Wood Science and Technology 47 (2013) 141–161.

[57] Z. Jalaludin, C. A. Hill, Y. Xie, H. W. Samsi, H. Husain, K. Awang, S. F. Curling, Analysis of the water vapour sorption isotherms of thermally modified acacia and sesendok, Wood Material Science and Engineering 5 (2010) 194–203.

[58] S. Brunauer, L. S. Deming, W. E. Deming, E. Teller, On a theory of the van der waals adsorption of gases, Journal of the American Chemical Society 62 (1940) 1723–1732.

[59] G. Almeida, J. O. Brito, P. Perre, Changes in wood-water relationship due to heat treatment assessed on micro-samples of three eucalyptus species, Holzforschung 63 (2009) 80–88.

[60] K. S. Sing, Reporting physisorption data for gas/solid systems with special reference to the determination of surface area and porosity (recommendations 1984), Pure and Applied Chemistry 57 (1985) 603–619.

[61] W. Pattaraprakorn, R. Nakamura, T. Aida, H. Niiyama, Adsorption of $CO_2$ and $N_2$ onto charcoal treated at different temperatures, Journal of Chemical Engineering of Japan 38 (2005) 366–372.

[62] A. Harding, N. Foley, P. Norman, D. Francis, K. Thomas, Diffusion barriers in the kinetics of water vapor adsorption/desorption on activated carbons, Langmuir 14 (1998) 3858–3864.

[63] P. Lodewyckx, The effect of water uptake in ultramicropores on the adsorption of water vapour in activated carbon, Carbon 48 (2010) 2549–2553.